

Multi-Window Time-Frequency Signature Reconstruction from Undersampled Continuous Wave Radar Measurements for Fall Detection

Branka Jokanovic, Moeness G. Amin, Yimin D. Zhang, and Fauzia Ahmad

Abstract

Fall detection is an area of increasing interest in independence-assisting remote monitoring technologies for the elderly population. Immediate assistance following a fall can lower the risk of medical complications, thus saving lives and reducing the associated health care costs. Therefore, it is important to detect a fall as it happens and promptly mobilize first responders for proper care and attendance to possible injury. Radar offers privacy and non-intrusive monitoring capabilities. Micro-Doppler signatures are typically employed for radar based human motion detections and classifications. Proper time-frequency signal representation is, therefore, required from which important features can be extracted. Missing or noise/interference corrupted data can compromise the integrity of micro-Doppler signatures and subsequently confuse the classifier. In this paper, we restore the time-frequency signatures associated with human motor activities, such as falling, bending over, sitting, and standing, by using a hybrid approach of compressive sensing and multi-window analysis based on Slepian or Hermite functions. Because time-frequency representations of many human gross-motor activities are sparse and share common support in joint-variable domains, the multiple measurement vector approach can be effectively applied for fall classification in both cases of full data or compressed observations.

Index Terms

Hermite functions, missing samples, multi-window time-frequency representation, multiple measurement vector, Slepian sequences, fall detection.

This paper is made possible by NPRP Grant # NPRP 6-680-2-282 from the Qatar National Research Fund (a member of Qatar Foundation). The statements made herein are solely the responsibility of the authors.

The authors are with the Center for Advanced Communications, Villanova University, Villanova, PA 19085, USA. E-mails: {branka.jokanovic, moeness.amin, yimin.zhang, fauzia.ahmad}@villanova.edu.

I. INTRODUCTION

Falls are one of the widely recognised risks encountered by the elderly in everyday life, be it in retirement homes or private residences. Various studies have shown that falling is the leading cause of fatal and nonfatal injuries among older adults, and the associated treatments result in high costs to the health care system [1], [2]. Thus, it is important to provide reliable and timely detection and classification of a fall when it occurs. Prompt assistance after a fall can reduce complications and save lives.

Radar is an effective noninvasive technology for providing self-dependent living to the elderly [3], [4]. This sensing modality has the capability to remotely detect various types of motions of animate and inanimate objects, such as humans and fans, in cluttered environments. Animate objects typically undergo translation in one, two, or three dimensions, whereas inanimate objects may assume rotational, vibrational, or oscillatory motions [5], [6]. Radar systems can be used as an effective sensing modality in both indoor and outdoor environments since they are insensitive to lighting conditions, can penetrate walls and fabrics, and operate in all types of weather conditions. However, analysis of the radar returns associated with animate and inanimate motions can be a demanding task, given their complex nature that stems from the presence of multiple signal components which correspond to various parts or limbs of the moving object [7], [8].

When dealing with radar measurements of human motions, two important spectral features can be observed. The first one is the Doppler effect, which is the frequency shift of the transmitted wave caused by the bulk target motion and it contains information about the target nominal velocity. The second feature is caused by the movement of various components of the body, including arms and legs. These motions generate sidebands about the Doppler frequency, referred to as micro-Doppler signatures. Since human motions inevitably change in time, a method for depicting the time-varying behavior of human motion is required.

Time-frequency representations (TFRs) are a powerful tool for the analysis of signals with time-varying spectra, including signals characterizing human motion. The simplest TFR is the short-time Fourier transform (STFT), which is obtained by applying a Fourier transform (FT) over a windowed signal. The square modulus of the STFT is the spectrogram. However, the resolution of spectrogram depends on the employed window size and shape, which limits its use. In order to overcome the drawback of a single-window spectrogram, different approaches

employing a set of windows have been introduced [9]-[16].

The set of optimal windows which provides maximum spectral concentration comprises the discrete prolate spheroidal sequences (DPSS) or Slepian sequences. DPSS can be defined as the eigenfunctions of a sinc kernel. As an alternative, Hermite functions, which are defined as eigenfunctions of the Fourier transform, can also be used. Hermite functions have several desirable properties, such as simplicity, recursion, and performance comparable to DPSS [17], [18]. These properties make them attractive for practical applications. Another set of windows is computed as eigenfunctions of a desirable time-frequency reduced interference kernel [14].

Irrespective of the number and types of windows, traditional time-frequency analysis fail to perform well when dealing with incomplete data. Recently, compressive sensing (CS), an approach that addresses the issue of missing samples, has become an area of growing interest [19]-[21]. Even though CS has been extensively examined in many areas, only a few researchers have addressed the sparsity in the time-frequency domain and the applications of sparse reconstruction techniques for accurate joint-variable representations of nonstationary signals [22]-[27].

In this paper, we consider the TFRs of specific human motions, namely, falling, bending over, sitting, and standing. We consider continuous-wave (CW) radar operation and assume the case when the measured radar signal has missing samples. This can be due to data multiplexing, hardware simplicity, or discarding of noise corrupted samples. In order to obtain a good estimate of the TFR, we use multiple windows while performing sparse reconstruction. The goal is to offer high energy signal concentration in the time-frequency plane. Additionally, we observe that the spectrograms corresponding to a set of windows, such as Slepian or Hermite functions, share similar support in the time-frequency domain. This property motivates the application of multiple measurement vector (MMV) model [28] for reconstruction of the corresponding multi-window TFR. The multi-window approach has recently provided effective TFRs with compressed observations [29], [30].

The remainder of the paper is organized as follows. In Section II, we present the CW radar signal model. We review the multi-window spectrogram and the definitions of various window functions in Section III, and discuss their advantages and shortcomings. The MMV approach for recovery of multi-window TFR is presented in Section IV. Section V analyzes experimental data corresponding to falling, bending over, sitting, and standing motions, collected with a CW radar in the Radar Imaging Lab at Villanova University. Conclusion is provided in Section VI.

II. CW RADAR SIGNAL MODEL

Consider a CW radar operating at frequency f_0 . The baseband radar return from a point target can be expressed as,

$$s(t) = \rho(t) \exp(-j\phi(t)), \quad (1)$$

where $\rho(t)$ and $\phi(t)$ are, respectively, the range-dependent amplitude and the phase of the return. If $R(t)$ is the law of motion of the target, then the phase is expressed as

$$\phi(t) = \frac{4\pi f_0 R(t)}{c} \quad (2)$$

where c is the speed of wave propagation in free-space. The associated Doppler frequency, $f_d(t)$, is determined by the derivative of the phase, $\phi(t)$, with respect to time, i.e.,

$$f_d(t) = -\frac{1}{2\pi} \frac{d\phi(t)}{dt} = -\frac{2f_0}{c} \frac{dR(t)}{dt}. \quad (3)$$

In contrast to the point target model in (1), the baseband return from an extended target, such as a human, can be considered as a sum of returns from a multiplicity of point scatterers comprising the target extent. As such, the corresponding Doppler signature is the superposition of the various component Doppler frequencies. Human motions typically produce time-varying Doppler frequencies, and the nature of the corresponding time-frequency signature is tied to the specific motion and shape of the target.

In this paper, we work with the discrete version of the baseband radar return in (1), given by

$$s(n) = s(t)|_{t=nT_s}, n = 0, 1, \dots, N - 1. \quad (4)$$

where T_s is the sampling period.

III. MULTI-WINDOW TIME-FREQUENCY REPRESENTATION

A multi-window spectrogram is defined as the weighted sum of L spectrograms corresponding to L different window functions [9]-[16]. In a discrete form, it can be expressed as,

$$P_{MW}(n, k) = \sum_{l=0}^{L-1} c_l(n) P_l(n, k), \quad (5)$$

where $c_l(n)$ is the weighting coefficient of the l th window function, whereas the l th spectrogram, $P_l(n, k)$, is obtained by applying the corresponding window function $\psi_l(n)$ to the discrete-time

signal $s(n)$ of length N and computing the FT of the windowed signal, followed by a magnitude squared operation, i.e.,

$$P_l(n, k) = \left| \sum_m s(n+m)\psi_l(m)e^{-j2\pi mk/N} \right|^2. \quad (6)$$

Different types of window functions can be employed for computing the multi-window spectrogram. We consider three sets of window functions described below, which can be used to enhance the time-frequency signal representation.

A. Slepian Sequences

Slepian sequences or DPSS are the optimal window functions that provide maximum spectral concentration for a given bandwidth B and time interval of length M . They are obtained by solving the problem of maximizing the energy concentration ν , which is defined as,

$$\nu = \frac{\sum_{m=0}^{M-1} |\psi^2(m)|}{\sum_{m=-\infty}^{\infty} |\psi^2(m)|}, \quad (7)$$

where $\psi(m)$ are the desired window functions. Slepian sequences can be computed as solutions of

$$\mathbf{C}\boldsymbol{\psi}_l = \nu_l\boldsymbol{\psi}_l, \quad (8)$$

where $\boldsymbol{\psi}_l = [\psi_l(0), \dots, \psi_l(M-1)]^T$ is the M -length eigenvector with $(\cdot)^T$ denoting transpose, and ν_l is the eigenvalue of matrix \mathbf{C} , whose (l, m) th element is given by

$$[\mathbf{C}]_{l,m} = \frac{\sin(2\pi B(l-m))}{\pi(l-m)}, \quad l, m \in \{0, 1, \dots, M-1\}. \quad (9)$$

B. Hermite Functions

Another set of window functions which can be used in multi-window time-frequency analysis is the set of Hermite functions. The Hermite functions of the zeroth and first orders are, respectively, defined as,

$$\psi_0(n) = \frac{1}{\sqrt[4]{\pi}} e^{-n^2/2}, \quad (10)$$

$$\psi_1(n) = \frac{\sqrt{2}n}{\sqrt[4]{\pi}} e^{-n^2/2}. \quad (11)$$

Higher order Hermite functions can be computed using recursion as

$$\psi_l(n) = n\sqrt{\frac{2}{l}}\psi_{l-1}(n) - \sqrt{\frac{l-1}{l}}\psi_{l-2}(n), \quad \forall l \geq 2. \quad (12)$$

A higher number of Hermite functions will provide better concentration in the time-frequency domain. For a signal $a(n)e^{j\theta(n)}$, the optimal value of L will depend on the order of signal phase laws. Additionally, if the magnitude $a(n)$ is constant over a window, i.e., $a(n) = a(n+m)$ for all m , then the weighting coefficients $c_l(n)$ can be considered constant [16]. In this paper, we assume constant values of the weighting coefficients.

C. Eigenvectors of a Time-Frequency Kernel

As another option, windows computed from a time-frequency kernel can be used. The premise of this method lies in the fact that most reduced interference distribution kernels, upon eigen-decomposition, are captured in the first few terms corresponding to the dominant eigenvalues. Each eigenterm forms a spectrogram with a window equal to the eigenvector. That is, in order to obtain the window functions, we compute the autocorrelation domain kernel, $\Upsilon(n, m)$, which is the FT of the ambiguity domain kernel, $\Omega(p, m)$, with respect to p , i.e.,

$$\Upsilon(n, m) = \sum_p \Omega(p, m) e^{-j2\pi pn/N}. \quad (13)$$

The windows are obtained as the eigenvectors of the rotated autocorrelation domain kernel. The rotated kernel can be defined using the unit-Jacobian linear transformation of variables,

$$\begin{bmatrix} n_1 \\ n_2 \end{bmatrix} = \begin{bmatrix} 1 & \frac{1}{2} \\ 1 & -\frac{1}{2} \end{bmatrix} \begin{bmatrix} n \\ m \end{bmatrix} \quad (14)$$

i.e., we can represent the rotated kernel as,

$$\tilde{\Upsilon}(n_1, n_2) = \Upsilon\left(\frac{n_1 + n_2}{2}, n_1 - n_2\right). \quad (15)$$

The eigenvectors of this kernel yield window functions ψ_l for time-frequency representation,

$$\tilde{\Upsilon} = \sum_{l=1}^L \beta_l \psi_l \psi_l^H, \quad (16)$$

where $(\cdot)^H$ denotes conjugate transpose.

For comparison, Fig. 1 demonstrates the first six window functions corresponding to DPSS, Hermite functions and eigenvectors of the time-frequency Choi-Williams kernel, respectively.

We observe that there is a resemblance between the three sets of window functions. The Slepian sequence is the optimal set when we know the signal bandwidth, whereas the Hermite functions can be used when there is no precise information available about the signal bandwidth, but the signal amplitude can be assumed constant within a window. The third type of windows is based on specific kernels, which are designed to remove cross-terms arising from multiple signal components. Thus, the resulting window sets for different kernel designs conform to different signal properties. In order to obtain a proper time-frequency signature, any prior information should be utilized when choosing the appropriate set of window functions.

By employing different windows and forming a multi-window spectrogram, we can significantly improve the signal energy concentration in the time-frequency domain. This is depicted in Fig. 2 for a signal representing a backward falling motion at an angle of 45 degrees relative to the radar. The signal is sampled at the Nyquist rate. Increasing the number of employed windows improves concentration. However, in most cases, a few dominant windows are sufficient for TFR estimation. This is evident from Fig. 2 where there is a negligible difference between the TFRs based on 5 and 7 windows. Thus, in the remainder of the paper, we will use 5 dominant window functions. In addition, since the Hermite functions and the windows computed from the time-frequency Choi-Williams kernel provide similar time-frequency signatures, we will focus on the Slepian and Hermite functions in the reconstruction of time-frequency signal representation and compare their performance in the sequel.

IV. MULTI-WINDOW TIME-FREQUENCY REPRESENTATION OF RANDOMLY UNDERSAMPLED MEASUREMENTS

In this section, we assume that a certain percentage of the N time samples of the baseband radar return $s(n)$ are missing. The randomly undersampled measurements can be represented as

$$x(n) = s(n) - v(n), \quad v(n) = \sum_{n_i} \delta(n - n_i) s(n), \quad (17)$$

where $\delta(\cdot)$ is the unit impulse, and n_i are the indices of the missing samples. The multi-window spectrogram of the undersampled signal vector $\mathbf{x} = [x(1), \dots, x(N)]^T$ using L window functions is given by,

$$P_{MW}(n, k) = \sum_{l=0}^{L-1} c_l \left| \sum_m (s(n+m) - v(n+m)) \psi_l(m) e^{-j2\pi km/N} \right|^2. \quad (18)$$

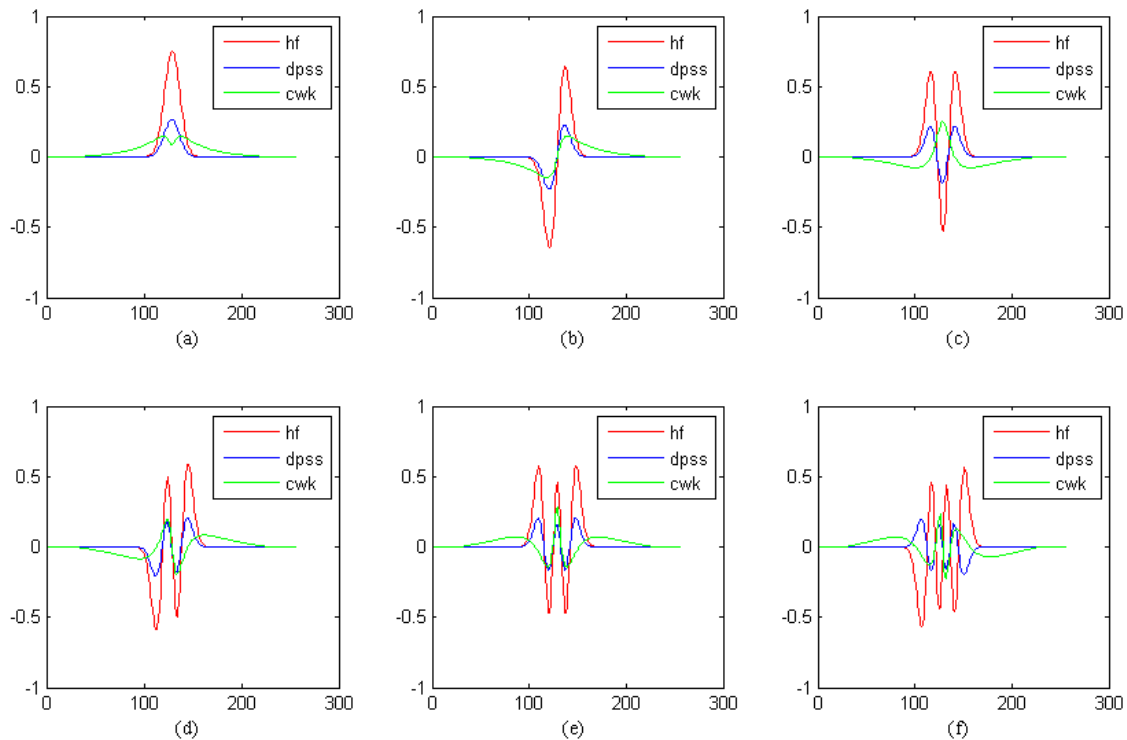


Fig. 1. DPSS, Hermite functions and windows obtained from time-frequency kernel. First six window functions are shown, i.e., from 0th to 5th order. (a) 0th order, (b) 1st order, (c) 2nd order, (d) 3rd order, (e) 4th order, (f) 5th order.

The missing samples in the time domain cause noise-like artifacts in the time-frequency domain, which clutter the resulting TFR [26]. Figs. 3, 4, 5 and 6 show the TFRs corresponding to different human motions, namely, fall backward, fall forward, sit/stand and bending over motions, respectively, when 50% of the samples are randomly missing. For comparison, the full data counterparts for the fall forward, sit/stands and bending over motion are also provided in Figs. 4, 5 and 6, whereas those for the fall backward case were provided in Fig. 2. We observe that the time-frequency signatures of human motions are significantly distorted due to the adverse effects of the missing samples and, therefore, cannot be employed for the recognition of human motor activities.

In order to reduce the artifacts and obtain a good estimate of the TFR, we utilize the sparse recovery approach. For the majority of nonstationary signals, their TFRs can be considered sparse since the energy is localized over a small bandwidth for a time slice. This property invites the application of sparse recovery methods for TFR estimation. More specifically, in case

of the multi-window spectrogram, we can observe that all spectrograms share similar support [29],[30]. The common support property can be incorporated in the problem at hand using the MMV model. More specifically, in solving L underdetermined systems of equations for L employed window functions, we incorporate the assumption of similar sparsity support. The MMV problem can be formulated as,

$$\mathbf{Y}_n = \mathbf{W}_n \mathbf{F}_n, \quad (19)$$

where $\mathbf{Y}_n = [\mathbf{y}_n^0, \dots, \mathbf{y}_n^{L-1}]$ and $\mathbf{F}_n = [\mathbf{f}_n^0, \dots, \mathbf{f}_n^{L-1}]$. Each column of \mathbf{Y} corresponds to the measurement vector obtained in the process of applying Hermite or Slepian function of the l th order. Namely, \mathbf{y}_n^l contains non-zero samples of windowed signal $x(n+m)\psi_l(m)$, whereas columns of \mathbf{F}_n are sparse vectors with a common sparse support. Using c_l , $l = 0, \dots, L-1$, as weighting coefficients, the weighted sum of these columns yields a multi-window TFR for time n . \mathbf{W}_n is a partial Fourier matrix and is the same for all $l = 0, \dots, L-1$, given time n . After obtaining \mathbf{f}_n^l , $\forall l$, we can estimate the multi-window TFR for each n , i.e., \mathbf{d}_n , as

$$\mathbf{d}_n = \sum_{l=0}^{L-1} c_l |\mathbf{f}_n^l|^2. \quad (20)$$

It is noted that the use of the multi-window approach in TFR provides two advantages over the single-window approach. First, the multi-window approach overcomes the poor resolution property of the single-window spectrogram. Second, multiple windows produce multiple measurement sets which improve the sparse vector estimation.

V. EXPERIMENTAL SETUP AND RESULTS

In this section, we evaluate the multi-window approach for sparse recovery of time-frequency signatures using real radar measurements of falling, bending over, sitting, and standing human motions. We compare the performance of sets of windows based on Slepian and Hermite functions.

A CW radar was set up in the Radar Imaging Lab at Villanova University. A vertically polarized horn antenna (BAE Systems, Model H-1479) with an operational frequency range of 1–12.4 GHz and 3-dB beamwidth of 45 degrees is used as a transceiver for the CW monostatic radar. The feed point of the antenna is positioned 1 m above the floor. Agilent's E5071B RF network analyzer is used for signal generation and measurement of radar returns. A carrier

frequency of 8 GHz is employed and the network analyzer is externally triggered at a 1 kHz sampling rate. The record time of each experiment is 10 seconds, resulting in a total of 10,000 data samples. The following five types of human motions are performed by two subjects at a distance of 3 m from the antenna feed point: 1) repeated sitting and standing, 2) bending over, 3) falling backward to the floor along the radar radiation direction, 4) falling forward to the floor along the radar radiation direction, and 5) falling backward to the floor at a 45° angle relative to the radar radiation direction.

We first downsample the data to the Nyquist sampling rate of 500 Hz, and the resulting signals are then randomly undersampled to create the incomplete data for processing. For classification purposes, the bending over and sit/stand motions are considered as the non-fall class, whereas the three types of falls are collectively considered as the fall class.

We compare and contrast the following sparsity based approaches for reconstruction of the TFR from incomplete data observations:

- 1) Single measurement vector (SMV) approach – This approach reconstructs the TFR by using a single Hamming window for each time n . Orthogonal matching pursuit (OMP) [21] is used as the reconstruction technique.
- 2) Separate reconstruction using multiple windows – This approach uses multiple windows, but does not impose similar sparsity support, i.e., each sparse vector is reconstructed independently by using OMP. We perform the reconstructions applying both Slepian and Hermite functions.
- 3) MMV approach – This is the approach described in Section IV where similar sparsity support is imposed in the reconstruction process. As in the previous case, we compute the TFRs using both Slepian and Hermite functions. The reconstruction is performed using the M-FOCUSS algorithm [28].

Figs. 7, 8 and 9 depict the TFR reconstruction results for fall, sit-and-stand and bending over motions, respectively, using the aforementioned methods when 50% of the samples are randomly missing. In the case of fall motion (Fig.7), we note that amongst all methods, the MMV approach (Figs. 7(d) and 7(e)) provides the least cluttered solutions. This is expected due to the imposed similar sparsity property. Also, both Slepian and Hermite functions exhibit similar performance in obtaining proper time-frequency representation. With regards to the reconstruction results for the sit/stand and bending over motions shown in Fig. 8 and Fig. 9, the difference between the

various methods is not significant due to the relatively simple structure of sitting, standing and bending over motions. However, the benefits of using the MMV approach are still noticeable when compared to the SMV and separate reconstruction approaches.

Next, we extract features from the TFRs reconstructed with the various methods and use a support vector machine (SVM) based classifier to discriminate between the fall and non-fall motions. SVM is a powerful tool for finding a hyperplane that separates the data classes and has been successfully used to differentiate various human gaits [31].

As can be seen from Figs. 7, 8 and 9, fall and non-fall motions have different time-frequency signatures. These differences can be used in determining prominent features which can distinguish fall from the non-fall motions. One feature which can be used for fall detection is the peak frequency [4]. The peak frequency distinguishes the fall from the sit/stand and bending over motions in the sense that falling generally assumes a higher absolute value as compared to the sit, stand and bending over. The peak frequency is defined as,

$$f_{peak} = \max[f_{max}, -f_{min}]. \quad (21)$$

In order to compare SMV, separate reconstruction, and MMV approaches, we follow the steps listed in Fig. 10. Similar framework was used in [3], [4]. After obtaining the TFR, denoted by matrix \mathbf{R} , we first localize the event. One way to this is by using the power burst curve (PBC) which is defined for each time slice as,

$$PBC(n) = \sum_{f_1}^{f_2} |R(n, k)|^2 + \sum_{-f_2}^{-f_1} |R(n, k)|^2. \quad (22)$$

where f_1 and f_2 denote the observed frequency range ($f_2 > f_1$). The following values can be used for the observed range, $f_1 = 30$ Hz and $f_2 = 180$ Hz. Usually, falls assume a high power content within a certain frequency range. An alternate metric for localizing an event is the center of gravity for each time slice as,

$$CoG(n) = \frac{\sum_k k |R(n, k)|}{\sum_k |R(n, k)|}. \quad (23)$$

The PBC measures the power within a certain frequency range, whereas the center of gravity is a weighted sum of the TFR values with the frequencies themselves being the weights. The center of gravity is a better measure of power spread since it favors higher frequency values and does not require *a priori* knowledge about the range of $[f_1, f_2]$.

After localizing an event, a 4-second window is formed around the event timing, within which the peak frequency is determined. A thresholding operation is used to remove clutter in the TFR which can cause false alarms. A set of ten thresholds is used to examine the changes in the detected peak frequency value and the resulting impact on the classification performance. The chosen threshold values range from 1% to 10% of the TFR maximum value. All the TFRs in Figs. 7, 8 and 9, which are obtained using the SMV and separate as well as MMV reconstruction approaches, contain clutter, whose effect is more evident for the SMV and separate reconstruction approaches. The clutter resembles salt-and-pepper noise and, thus, complicates the extraction of the peak frequency feature. Image processing techniques, such as median filtering [32], can be used for clutter reduction before applying the thresholding, feature extraction, and classification procedures. A 7×7 median filter is applied to the TFRs obtained using the SMV and separate reconstruction methods before the features are extracted.

We have 32 data sets for the fall events and 32 data sets for the non-fall events. In the training process, 6 fall signals are used as fall events whereas 3 sit-and-stand and 3 bending-over signals are used as non-fall events. The remaining 26 fall and 26 non-fall signals are used for the testing process. For each method, by changing the threshold value, true positive and false positive rates are evaluated. The resulting classification performance in terms of the receiver operating characteristics (ROC) curves [33] is depicted in Fig. 11. Each ROC curve corresponds to one considered approach and it shows the true positive rate versus the false alarm rate. The performance of a specific method can be measured by computing the area under the ROC curve (AROC), which is also specified for each approach in Fig. 11. It is evident that the MMV approach using the Slepian sequence provides the highest AROC value, thus demonstrating its superiority for fall detection over other methods in the case of missing samples.

VI. CONCLUSION

In this paper, the time-frequency signal representation of human motions was estimated from observed data with missing samples for the purpose of elderly fall detection. We used multi-window spectrogram approach based on Slepian and Hermite functions in conjunction with sparse signal recovery techniques that exploit the multiple measurement vector model to achieve high energy localization and enhanced sparsity in the time-frequency domain. In order to validate the proposed approach, we reconstructed time-frequency representations with real data under

missing samples and performed classification of the resulting radar signatures corresponding to fall, sit/stand, and bending-over motions. It was shown that the proposed technique achieves a high classification accuracy, with the discrete prolate spheroidal sequences slightly outperforming the Hermite functions.

REFERENCES

- [1] X. Yu, "Approaches and principles of fall detection for elderly and patient," in *IEEE Int. Conf. HealthCom*, Singapore, July 2008, pp. 42–47.
- [2] I. Immoreev and T.-H. Tao, "UWB radar for patient monitoring," *IEEE Aerospace and Electronic Systems Magazine*, vol. 23, no. 11, pp. 11–18, 2008.
- [3] L. Liu, M. Popescu, M. Skubic, M. Rantz, T. Yardibi, and P. Cuddihy, "Automatic fall detection based on Doppler radar motion signature," in *PervasiveHealth 2011*, pp. 222–225.
- [4] L. Ramirez Rivera, E. Ulmer, Y. D. Zhang, W. Tao, and M. G. Amin, "Radar-based fall detection exploiting time-frequency features," in *Proc. IEEE China Summit and Int. Conf. Signal and Inf. Process.*, Xi'an, China, July 2014.
- [5] M. I. Skolnik, *Radar Systems*. McGraw Hill, 2001.
- [6] P. Setlur, M. Amin, and F. Ahmad, "Analysis of micro-doppler signals using linear fm basis decomposition," in *Proc. SPIE*, vol. 6210, Orlando, FL, April 2006.
- [7] C. Clemente, A. Balleri, K. Woodbridge, and J. J. Soraghan, "Developments in target micro-doppler signatures analysis: radar imaging, ultrasound and through-the-wall radar," *EURASIP Journal on Advances in Signal Processing*, vol. 2013, no. 1, pp. 1–18.
- [8] V. C. Chen, "Analysis of radar micro-doppler with time-frequency transform," in *Proc. IEEE Workshop on Stat. Signal and Array Process.*, Pocono Manor, PA, Aug. 2000, pp. 463–466.
- [9] M. Bayram and R. G. Baraniuk, "Multiple window time-frequency and time-scale analysis," in *Proc. SPIE*, 1996, pp. 174–185.
- [10] F. Cakrak and P. J. Loughlin, "Multiple window non-linear time-varying spectral analysis," in *Proc. IEEE ICASSP*, vol. 4, 1998, pp. 2409–2412.
- [11] G. Fraser and B. Boashash, "Multiple window spectrogram and time-frequency distributions," in *Proc. IEEE ICASSP*, vol. 4, 1994, pp. IV–293.
- [12] M. Hansson, "Multiple window decomposition of time-frequency kernels using a penalty function for suppressed sidelobes," in *Proc. IEEE ICASSP*, Toulouse, France, May 2006, pp. 2883–2886.
- [13] W. J. Williams and S. Aviyente, "Optimum window time-frequency distribution decompositions," in *Proc. Asilomar Conf.*, vol. 1, Pacific Grove, CA, Nov. 1998, pp. 817–821.
- [14] M. G. Amin, "Spectral decomposition of time-frequency distribution kernels," *IEEE Trans. Signal Process.*, vol. 42, no. 5, pp. 1156–1165, 1994.
- [15] J. W. Pitton, "Time-frequency spectrum estimation: An adaptive multitaper method," in *Proc. IEEE-SP Int. Symp. Time-Frequency and Time-Scale Analysis*, Pittsburgh, PA, Oct. 1998, pp. 665–668.
- [16] F. Çakrak and P. J. Loughlin, "Multiwindow time-varying spectrum with instantaneous bandwidth and frequency constraints," *IEEE Trans. Signal Process.*, vol. 49, no. 8, pp. 1656–1666, 2001.

- [17] Y. Xu, S. Haykin, and R. J. Racine, "Multiple window time-frequency distribution and coherence of EEG using Slepian sequences and Hermite functions," *IEEE Trans. Bio. Engin.*, vol. 46, no. 7, pp. 861–866, 1999.
- [18] I. Orović, N. Žarić, S. Stanković, and M. Amin, "A multiwindow time-frequency approach based on the concepts of robust estimate theory," in *Proc. IEEE ICASSP*, Prague, Czech Republic, May 2011, pp. 3584–3587.
- [19] E. J. Candès and M. B. Wakin, "An introduction to compressive sampling," *IEEE Signal Process. Magazine*, vol. 25, no. 2, pp. 21–30, 2008.
- [20] D. L. Donoho, "Compressed sensing," *IEEE Trans. Inf. Theory.*, vol. 52, no. 4, pp. 1289–1306, 2006.
- [21] J. A. Tropp and A. C. Gilbert, "Signal recovery from random measurements via orthogonal matching pursuit," *IEEE Trans. Inf. Theory*, vol. 53, no. 12, pp. 4655–4666, 2007.
- [22] P. Flandrin and P. Borgnat, "Time-frequency energy distributions meet compressed sensing," *IEEE Trans. Signal Process.*, vol. 58, no. 6, pp. 2974–2982, 2010.
- [23] M. G. Amin, *Compressive Sensing for Urban Radar*. CRC Press, 2014.
- [24] L. Stankovic, I. Orovic, S. Stankovic, and M. Amin, "Compressive sensing based separation of nonstationary and stationary signals overlapping in time-frequency," *IEEE Trans. Signal Process.*, vol. 61, no. 18, pp. 4562–4572, Sept 2013.
- [25] B. Jokanović, M. Amin, and S. Stanković, "Instantaneous frequency and time-frequency signature estimation using compressive sensing," in *Proc. SPIE*, vol. 8714, Baltimore, MD, May 2013.
- [26] Y. D. Zhang, M. G. Amin, and B. Himed, "Reduced interference time-frequency representations and sparse reconstruction of undersampled data," in *Proc. European Signal Proc. Conf.*, Marrakech, Morocco, Sept. 2013.
- [27] L. Stankovic, S. Stankovic, and M. Amin, "Missing samples analysis in signals for applications to L-estimation and compressive sensing," *Signal Processing*, vol. 94, pp. 401–408, 2014.
- [28] S. F. Cotter, B. D. Rao, K. Engan, and K. Kreutz-Delgado, "Sparse solutions to linear inverse problems with multiple measurement vectors," *IEEE Trans. Signal Process.*, vol. 53, no. 7, pp. 2477–2488, 2005.
- [29] M. G. Amin, Y. D. Zhang, and B. Jokanović, "Time-frequency signature reconstruction from random observations using multiple measurement vectors," in *Proc. IEEE ICASSP*, Florence, Italy, May 2014.
- [30] B. Jokanović, M. G. Amin, and Y. D. Zhang, "Reconstruction of multi-window time-frequency representation based on Hermite functions," in *Proc. SPIE*, Baltimore, MD, May 2014.
- [31] Y. Kim and H. Ling, "Human activity classification based on micro-Doppler signatures using a support vector machine," *IEEE Trans. Geosci. Remote Sens.*, vol. 47, no. 5, pp. 1328–1337, 2009.
- [32] T. Huang, G. Yang, and G. Tang, "A fast two-dimensional median filtering algorithm," *IEEE Trans. Acoust., Speech, Signal Proc.*, vol. 27, no. 1, pp. 13–18, 1979.
- [33] T. Fawcett, "An introduction to ROC analysis," *Pattern Recognition Letters*, vol. 27, no. 8, pp. 861–874, 2006.

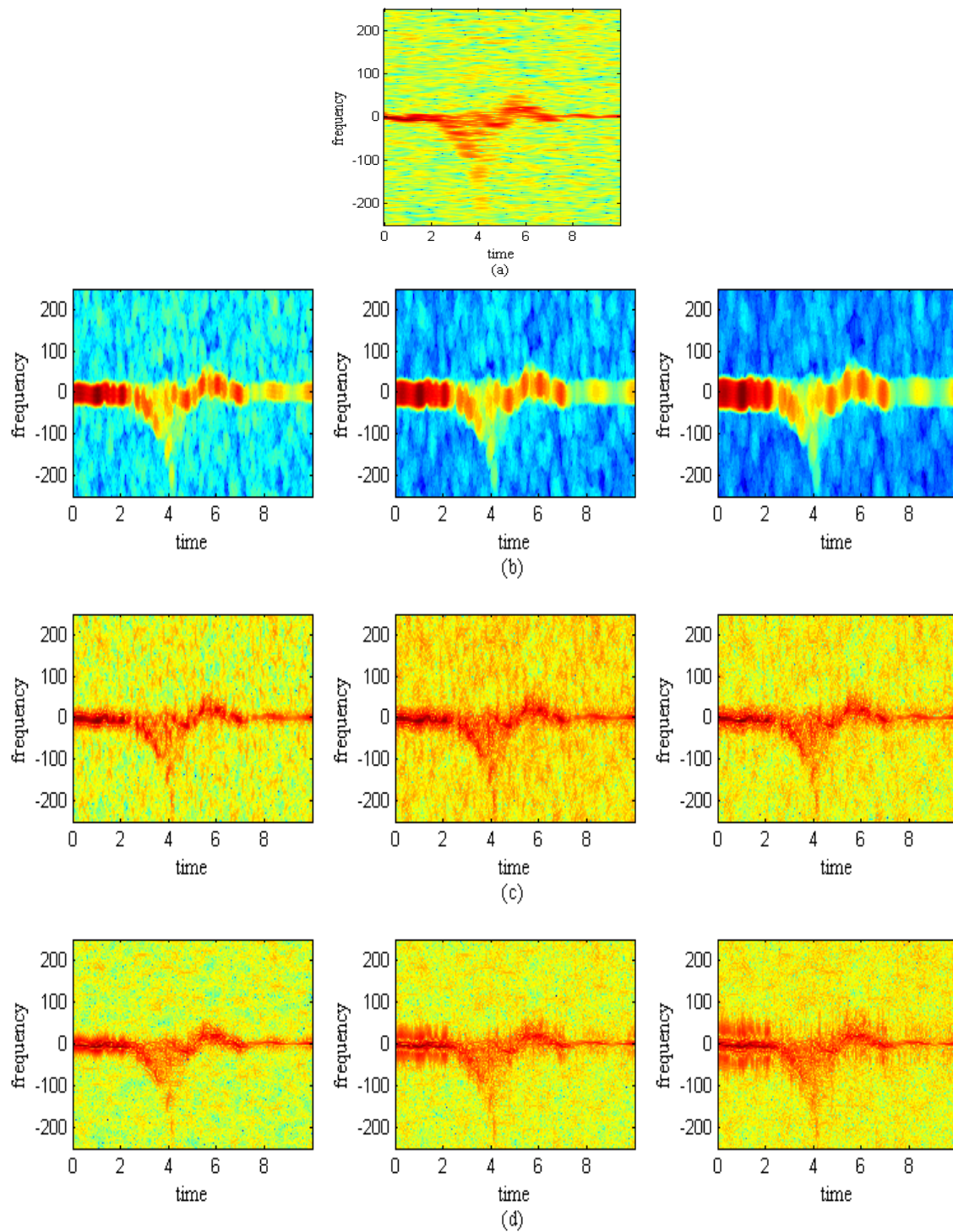


Fig. 2. TFRs obtained using different number of window functions: (a) Spectrogram using 256-point Hamming window, (b) multi-window spectrogram obtained using 3, 5 and 7 DPSS functions, respectively, (c) multi-window spectrogram obtained using 3, 5 and 7 Hermite functions, respectively, (d) multi-window spectrogram obtained using first 3, 5 and 7 dominant time-frequency kernel eigenvectors, respectively.

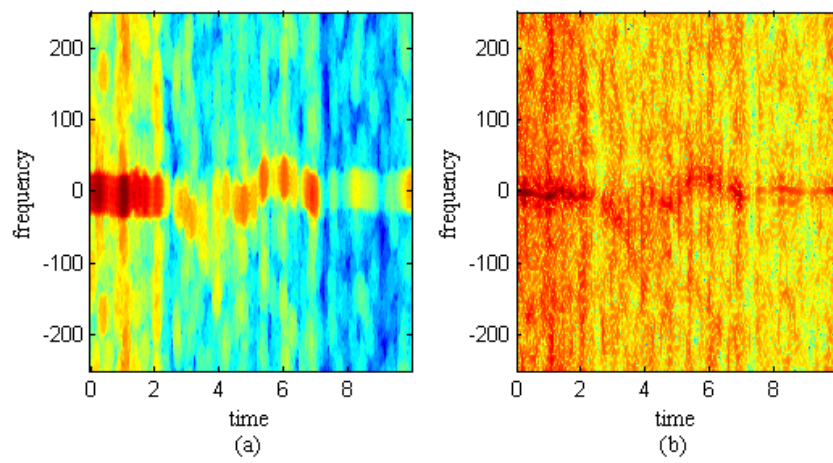


Fig. 3. Multi-window spectrogram of data representing a fall backward with 45 degrees. 50% of samples are missing, and 5 window functions are employed. (a) Incomplete data with DPSS (b) Incomplete data with Hermite functions.

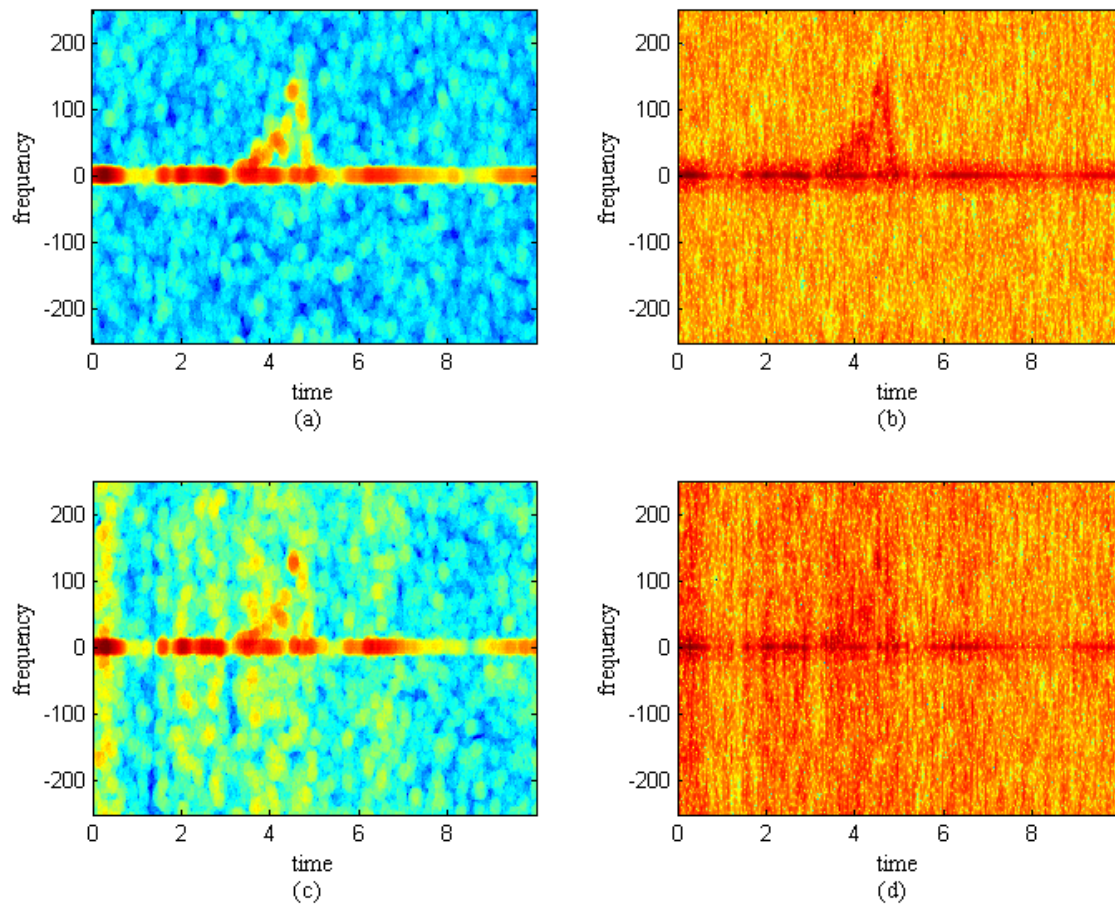


Fig. 4. Multi-window spectrogram of data representing a fall forward with 0 degrees. 50% of samples are missing, and 5 window functions are employed. (a) Full data with DPSS, (b) Full data with Hermite functions, (c) Incomplete data (50% missing) with DPSS, (d) Incomplete data (50% missing) with Hermite functions.

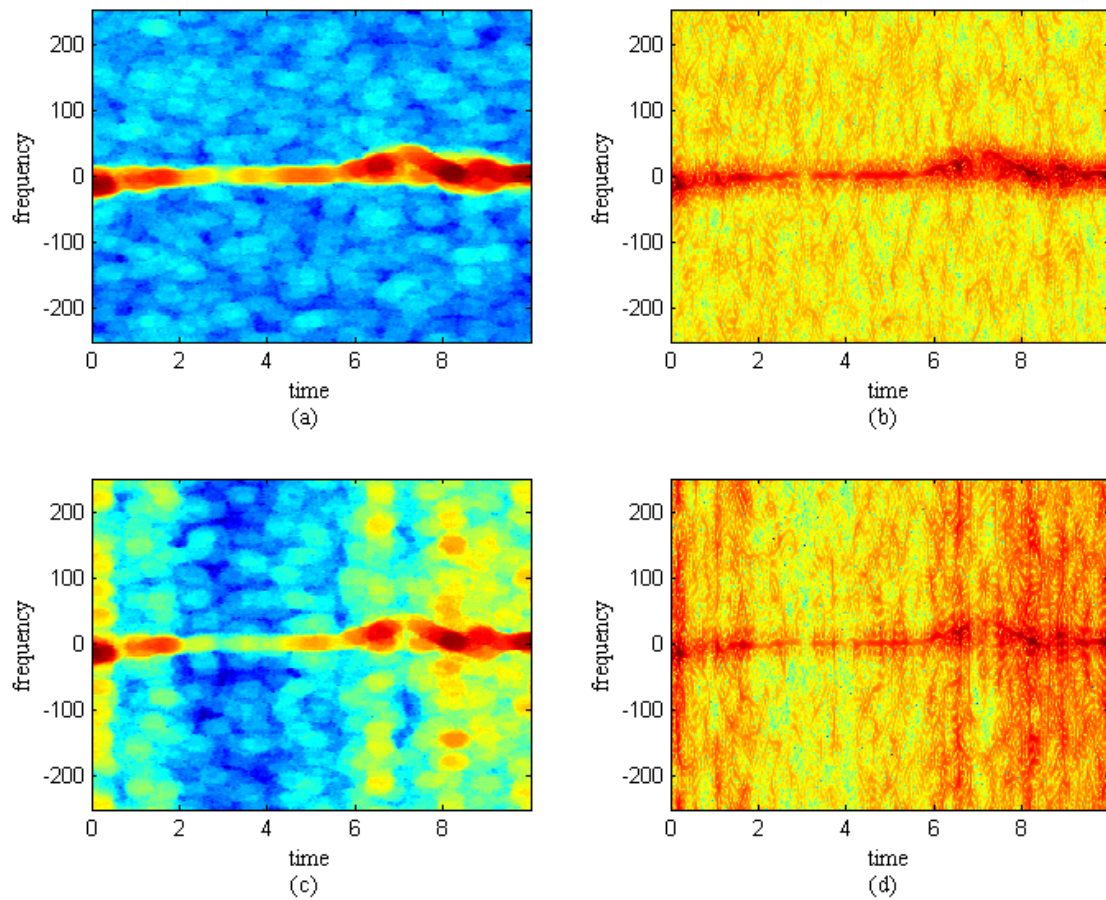


Fig. 5. Multi-window spectrogram of data representing a sit/stand motion using 5 window functions, (a) Full data with DPSS, (b) Full data with Hermite functions, (c) Incomplete data (50% missing) with DPSS, (d) Incomplete data (50% missing) with Hermite functions.

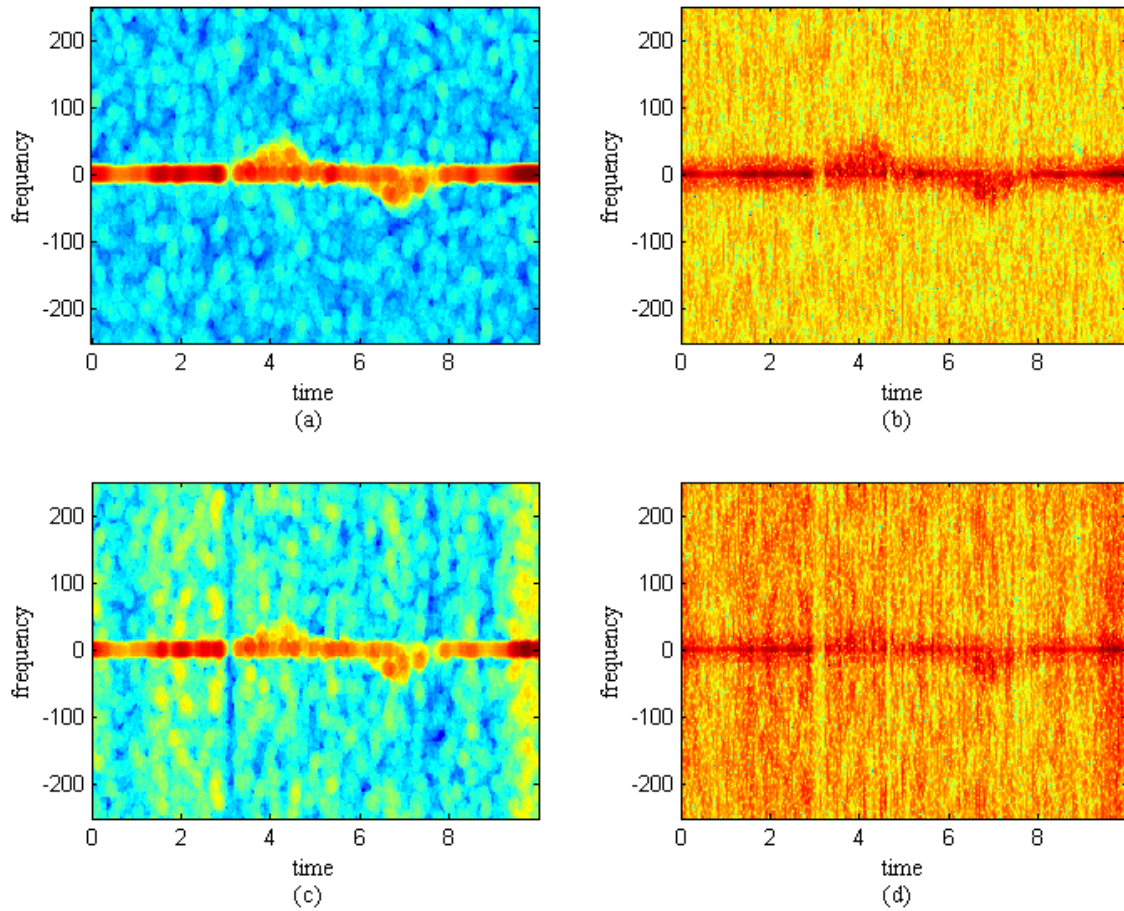


Fig. 6. Multi-window spectrogram of data representing a bending over motion using 5 window functions, (a) Full data with DPSS, (b) Full data with Hermite functions, (c) Incomplete data (50% missing) with DPSS, (d) Incomplete data (50% missing) with Hermite functions.

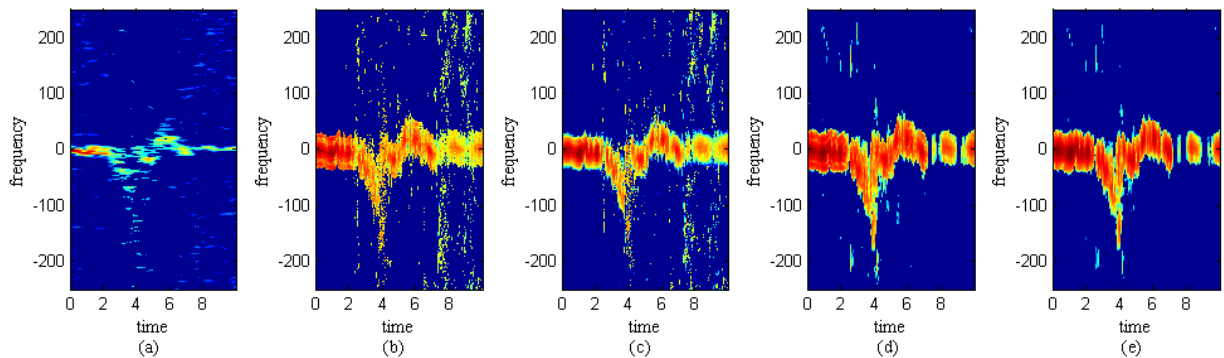


Fig. 7. Reconstruction results for signal representing a backward fall with 45 degrees. 50% of samples are randomly missing. (a) SMV approach, (b) Separate reconstruction using 5 DPSS windows, (c) Separate reconstruction using 5 Hermite windows, (d) MMV approach using 5 DPSS windows, (e) MMV approach using 5 Hermite windows.

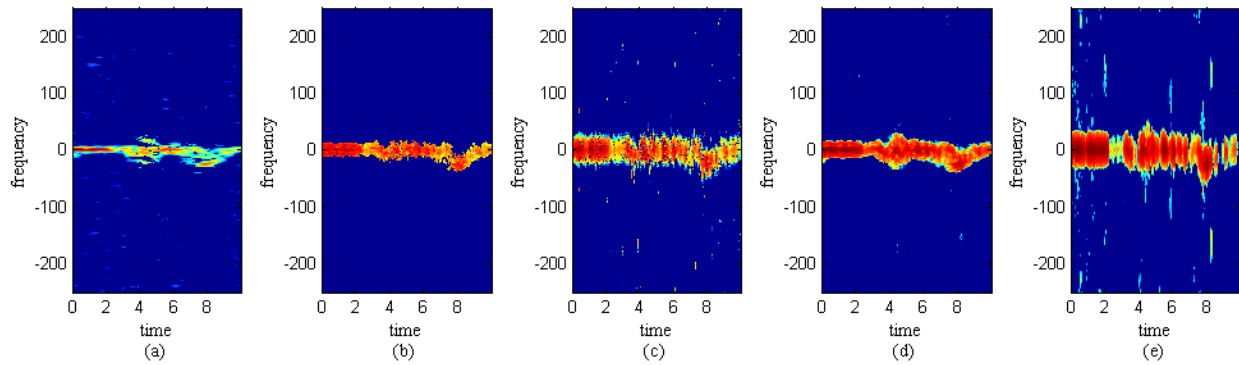


Fig. 8. Reconstruction results for signal representing a sit/stand motion. 50% of samples are randomly missing. (a) SMV approach, (b) Separate reconstruction using 5 DPSS windows, (c) Separate reconstruction using 5 Hermite windows, (d) MMV approach using 5 DPSS windows, (e) MMV approach using 5 Hermite windows.

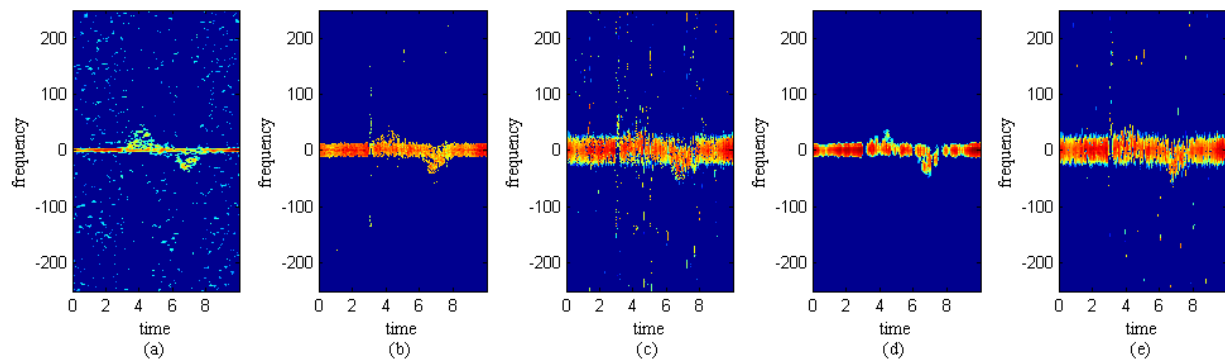


Fig. 9. Reconstruction results for signal representing a bending over motion. 50% of samples are randomly missing. (a) SMV approach, (b) Separate reconstruction using 5 DPSS windows, (c) Separate reconstruction using 5 Hermite windows, (d) MMV approach using 5 DPSS windows, (e) MMV approach using 5 Hermite windows.

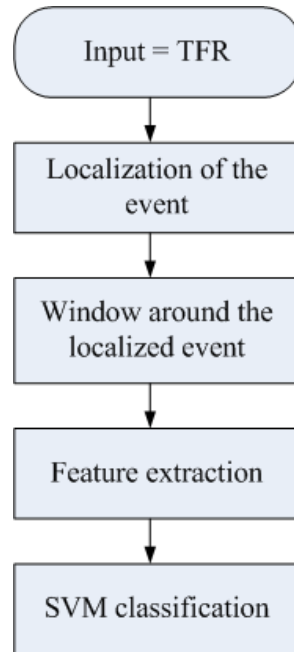


Fig. 10. Diagram showing the steps used in the process of classification.

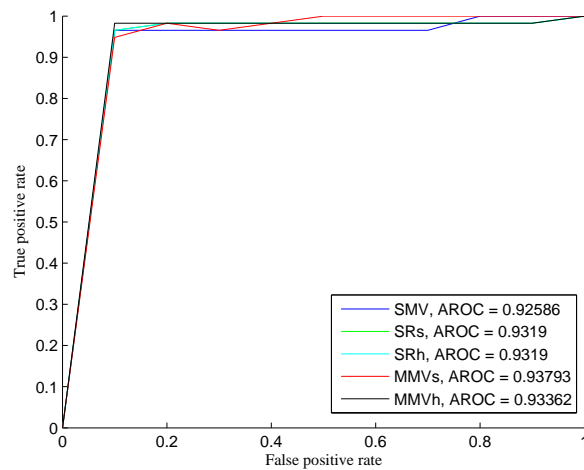


Fig. 11. ROC curves for the described methods. SR indicates separate reconstruction results. Subscript 's' denotes the use of Slepian sequence, whereas 'h' indicates Hermite sequence. AOC values are also depicted for each curve.